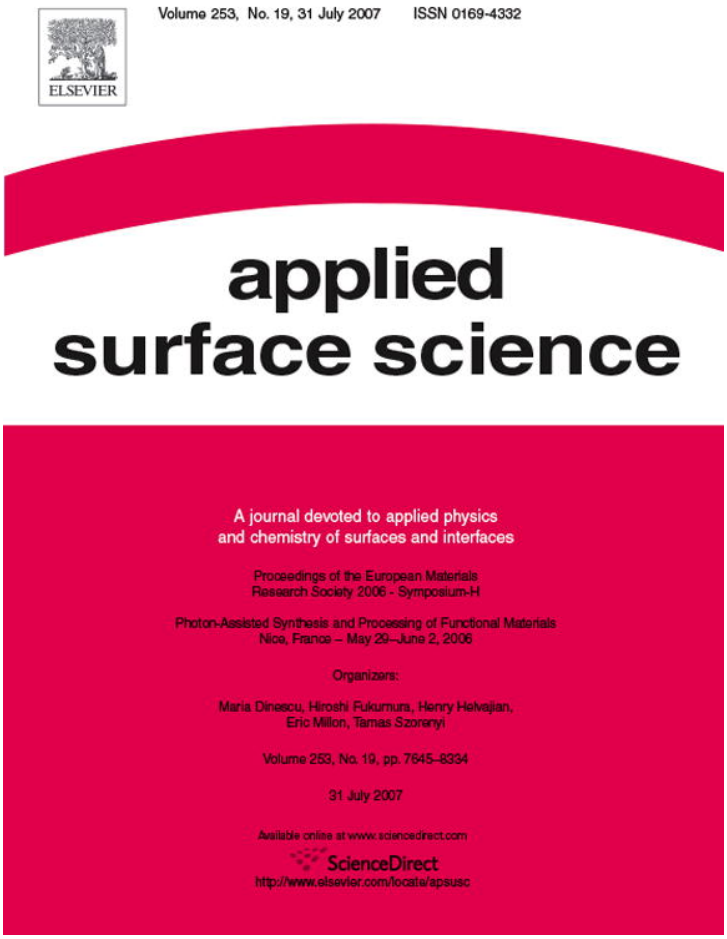

Available online at www.sciencedirect.com
ScienceDirect
Applied Surface Science 253 (2007) 7686–7691
applied surface science
www.elsevier.com/locate/apsusc

Modeling of plasma-controlled surface evaporation and condensation of Al target under pulsed laser irradiation in the nanosecond regime

V.I. Mazhukin [a], V.V. Nossov [a], I. Smurov [b,*]

[a] *Institute of Mathematical Modeling of RAS, 4a Miusskaya sqr., 125047 Moscow, Russia*
[b] *Ecole Nationale d'Ingénieurs de Saint-Etienne (ENISE), DIPI Laboratory, 58 rue Jean Parot, 42023 Saint-Etienne Cedex 2, France*

Available online 20 February 2007

Abstract

Phase transition on the surface of an aluminium target and vapour plasma induced by laser irradiation in the nanosecond regime at the wavelengths of 1.06 and 0.248 μm with an intensity of 10^8–10^9 W/cm^2 in vacuum are analysed. Particular attention is paid to the wavelength dependence of the observed phenomena and the non-one-dimensional effect caused by the Gaussian laser intensity distribution. A transient two-dimensional model is used which includes conductive heat transfer in the condensed phase, radiative gas dynamics and laser radiation transfer in the plasma as well as surface evaporation and back condensation at the phase interface. It is shown that distinctions in phase transition dynamics for the 1.06 and 0.248 μm radiation result from essentially different characteristics of the laser-induced plasmas. For the 1.06 μm radiation, evaporation stops after the formation of hot optically thick plasma, can occasionally resume at a later stage of the pulse, proceeds non-uniformly in the spot area, and the major contribution to the mass removal occurs in the outer part of the irradiated region. Plasma induced by the 0.248 μm laser is much more transparent therefore evaporation does not stop but continues in the subsonic regime with the Mach number of about 0.1.

Keywords: Surface phase transitions; Laser-plasma interaction; Knudsen layer

1. Introduction

The technique of material removal from a condensed target by the action of short high-power laser pulses usually referred to as *laser ablation* (LA) forms the basis for a number of technologies such as pulsed laser deposition (PLD), micro-machining, structuring or analysis of solid materials [1–3]. Along with the intensity and the pulse duration, the wavelength of laser radiation is a key parameter providing great flexibility to tailor this technique to suit specific tasks.

For metal targets, surface evaporation is always an important mechanism of material removal [1,4]. The process is characterized by the formation of a sharp phase boundary between the condensed and vapour phases and of a transient non-equilibrium layer adjacent to the boundary referred to as the Knudsen layer (KL) [5–7]. The degree of non-equilibrium (the intensity) of evaporation is conveniently characterized by the Mach number on the outer boundary of the KL. Upon irradiation with a constant intensity in vacuum or in an environmental gas with a low counter-pressure, evaporation proceeds with a sonic velocity $Ma = 1$ [4,8]. Generally, subsonic evaporation $Ma < 1$ is realized because of the counter-pressure of the external gaseous medium or the previously vaporized material [9–11]. Recently, the problem of back condensation to the irradiated surface (the process opposite to surface evaporation) has been the concern of a number of studies analysing laser ablation [12–14].

The course of laser-induced evaporation changes qualitatively if a plasma is formed in the evaporated matter. The most well-known consequence of the plasma formation is the absorption of incident laser radiation (screening effect) that affects the target heating and evaporation rate [14–18]. A much less studied result of the plasma formation is the generation of a high counter-pressure: as it was demonstrated [19–21], high pressure of the plasma cannot only decelerate but reverse the

* Corresponding author. Tel.: +33 4 77 91 01 61; fax: +33 4 77 43 84 99.
E-mail address: smurov@enise.fr (I. Smurov).

0169-4332/$ – see front matter © 2007 Elsevier B.V. All rights reserved.
doi:10.1016/j.apsusc.2007.02.039

direction of the phase transition, and leads to the back condensation onto the surface during the laser pulse. Intensity thresholds for plasma formation, plasma characteristics (absorption mechanisms, transparency, temperature, pattern structure) and its effect on phase transition are known to be dependent on laser wavelength [3,22,23].

The main objective of the present study is a comparative analysis of the plasma-controlled phase transition on the surface of an aluminium target induced by nanosecond laser radiation at the wavelengths of 1.06 and 0.248 μm with an intensity of 10^8–10^9 W/cm^2 in vacuum.

2. Problem statement

The physical model used in this paper was described previously [20,21] and accounts for the following phenomena: (i) surface heating of a metal target by laser radiation and conductive heat transfer; (ii) surface evaporation and back condensation; (iii) transfer and absorption of laser radiation in vapour plasma; (iv) gas-dynamic expansion, heating and ionisation of the plasma; (v) generation and transfer of thermal radiation, Fig. 1(a). The processes were mathematically described in a cylindrical coordinate system co-moving with the target surface. Its origin was located in the centre of the laser beam, the r-axis coincided with the surface, and the z-axis was directed along the outward drawn normal, Fig. 1(b).

2.1. Condensed medium

In the region $0 < r < L_r$, $-l_z < z < 0$ occupied by a condensed medium, Fig. 1(b), the heat transfer was described by the heat conduction equation. The model did not account for the target melting that affects insignificantly the surface phase transitions in the considered irradiation regimes and for the hydrodynamic phenomena in the melt that would substantially complicate the model of the condensed medium and the computational algorithm.

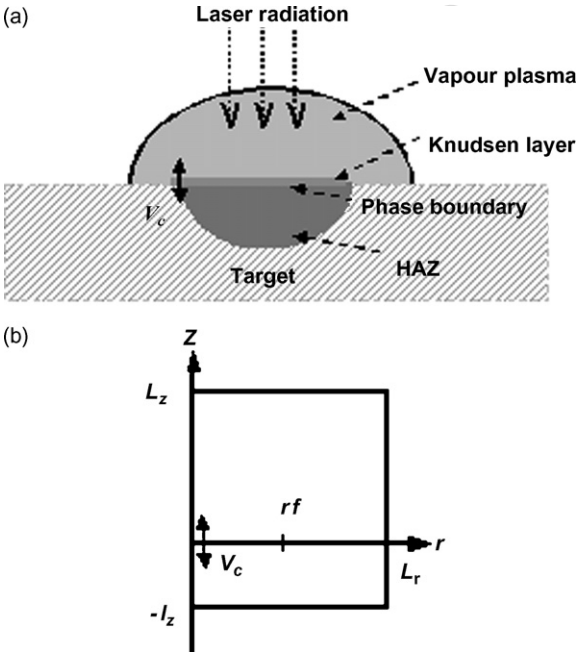

Fig. 1. Set-up (a) and reference frame (b) of the problem.

2.2. Gaseous medium and plasma

The processes in the vapour region $0 < r < L_r$, $0 < z < L_z$, Fig. 1(b), were described by a system of radiative gas dynamics equations and the laser radiation transfer equation [20,24]: the movement of the vapour plasma was treated in the compressible non-viscous non-heat conductive gas approximation; the energy balance equation accounted for the work of pressure, heating by the laser and thermal radiation; the thermal radiation transfer was described in P_1 (diffusion) approximation; the laser radiation transfer equation along the z-axis took into account both the component incident on the target and the reflected one. Plasma absorption coefficients for thermal and laser radiation were calculated by the approach of Ref. [25] with the equilibrium charge composition and the excited state distribution of the plasma determined by the Saha–Boltzmann equations [26].

2.3. Interface boundary conditions

Boundary conditions at the interface $z = 0$, Fig. 1(b) relate six quantities: the front velocity V_c, the temperature T_c and the pressure P_c of the target surface with the temperature T, the density ρ and the normal velocity v in the plasma at the external boundary of the KL. The conditions are formulated in different ways for the evaporation and condensation [7]. Independently of the direction of the phase transition the three conservation laws are fulfilled:

$$\lambda_c \frac{\partial T_c}{\partial z} = AG^- + L_v \rho_c V_c, \qquad \rho_c V_c = \rho(V_c - v),$$
$$\rho_c V_c^2 + P_c = \rho(V_c - v)^2 + P, \tag{1}$$

where L_v is the heat of evaporation, λ the thermal conductivity, G^- the incident laser flux and A is the surface absorptivity. It is seen from the energy balance relation that the laser heating of the target is described by the so-called surface approximation.

In the case of evaporation, two additional relationships of the Crout model were used [20,21]: $T/T_c = f_1(Ma)$, $\rho/\rho_{sat} = f_2(Ma)$, ρ_{sat} is the saturated vapour density. The system of boundary conditions has one free parameter: the Mach number Ma, that was assumed to be not greater than unity [5–7].

On reaching the inequality $P_{sat} < P$ with P_{sat} being the saturated vapour pressure the phase transition changes direction and evaporation is replaced by condensation $Ma < 0$ that may take place in both the subsonic and supersonic regimes [7]. In the case of subsonic condensation $-1 < Ma < 0$, only one additional relationship was used [20,21]: $P/P_{sat} = 0.95 \exp(2.42|Ma|)$, that approximates the tabular function $F_s(T/T_c, Ma) = P/P_{sat}$ [27] and neglects the rather weak dependence of the F_s on the temperature ratio. For the supersonic regime $Ma < -1$, $P/P_{sat} > 10$ all the three fluid parameters at the KL were determined by extrapolation [7,20,21].

2.4. Algorithm of numerical solution

The differential model was solved by the finite difference (FD) technique. The heat conduction equation with a convective term and temperature-dependent coefficients was approximated by a fully implicit difference scheme and was solved by the alternating direction method [28]. A detailed description of the technique used to solve radiative gas dynamics equations is given in Ref. [29].

3. Results and discussion

In this section regularities of the phase transitions induced by the 1.06 and 0.248 μm lasers with a fixed pulse duration $\tau = 20$ ns, the beam radius $r_f = 250$ μm and the peak intensity G_0 within a range of 10^8–10^9 W/cm^2 are compared. The intensity is assumed to have a Gaussian distribution in time and space:

$$G^-(t, r, z = L_z) = G_0 \exp\left(-\left(\frac{r}{r_f}\right)^2\right) \exp\left(-4\left(\frac{t}{\tau} - 1\right)^2\right). \quad (2)$$

Parameters of the aluminium used in calculations were taken from Ref. [30] and different values of the thermal conductivity, heat capacity and density were used in the temperature ranges $T_c < T_m$ and $T_c > T_m$, T_m is the melting temperature [20,21]. The background density in the gaseous region of 3×10^{-6} g/cm^3 was taken that corresponds to the background pressure of 2×10^{-3} bar.

The surface absorptivity A at high temperatures is only very approximately known (≈60–70% for 0.308 μm radiation [3], ≈40–50% for 1.06 μm [15]) and is much higher than the absorptivity of cold aluminium (≈5–10% for 0.2–1 μm [3,31]). To better clarify the phenomenon of the plasma properties dependence on wavelength, the surface absorptivity was assumed to be independent of the laser wavelength and was approximated as follows: $A(T_c > T_m) = 0.64(T_c/11600)^{0.4}$, $A(T_c < T_m) = A(T_m) = 0.231$ [15]. Possible variation of A leads to a proportional variation of the absorbed energy flux AG^- and results in a shift in predictions of the model in respect of the pulse intensity G_0.

3.1. Optical characteristics of plasma

The transmission coefficient is one of the most important optical characteristics of a plasma: it shows which part of the laser energy reaches the target and is spent for heating and removal of the material. Fig. 2 represents time dependencies of this quantity $T_{pl} = G^-(r, z = 0)/G^-(r, z = L_z)$ taken in the beam centre $r = 0$ for the 1.06 and 0.248 μm radiation with $G_0 = 5 \times 10^8$ W/cm^2. The dashed lines in the figures indicate the action time and the shape of the laser pulse. For the 1.06 μm radiation the vapour remains transparent for some time after the onset of evaporation. A sharp decrease of the transmission occurs at the instant $t^* \approx 17$ ns with a minimum value of about 3% and corresponds to the initiation of the plasma. For the

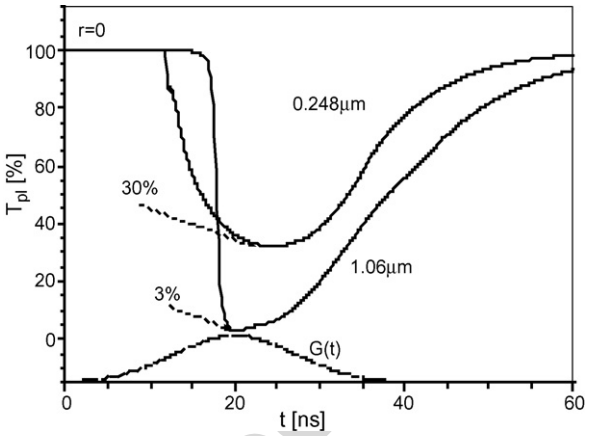

Fig. 2. Evolution of the plasma transmission $T_{pl}(t, r) = G^-(t, r, z = 0)/G^-(t, r, z = L_z)$ in the beam centre $r = 0$ for the laser wavelength of 1.06 and 0.248 μm, $G_0 = 5 \times 10^8$ W/cm^2. Dashed line indicates the laser pulse shape.

0.248 μm radiation the picture is substantially different: the decrease of the transmission begins just after the onset of evaporation at $t^* \approx 10$ ns but even at its minimum the coefficient does now fall below 30%. The observed distinctions of IR and UV laser-induced plasmas are consistent with the data of a comparative review given in Ref. [3].

Dependence of the analysed phenomena on laser wavelength is explained by the difference between the plasma absorption coefficient $\kappa = \kappa(\lambda, T, \rho)$ in the IR and UV ranges. Two curves of this quantity calculated for the laser wavelength $\lambda = 1.06$ and 0.248 μm at the fixed density $\rho = 5 \times 10^{-3}$ g/cm^3 are shown in Fig. 3. For the 1.06 μm wavelength the inverse bremsstrahlung is the only absorption mechanism, and its contribution increases monotonically with temperature owing to the increase of the equilibrium concentration of electrons. For the 0.248 μm radiation the dependence is more complicated and includes the contribution of both the inverse bremsstrahlung and the photo-ionisation: it increases in the temperature range $T < 1$ eV in which the photo-ionisation of neutral atoms dominates and diminishes for higher temperatures because nearly all neutrals are already ionised. The comparison of the two curves shows

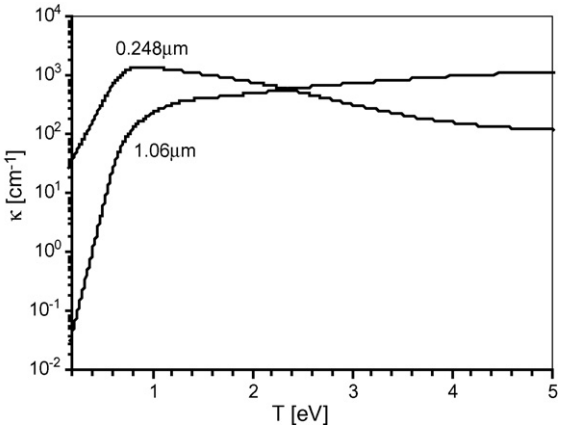

Fig. 3. Temperature dependency of plasma absorption coefficient $\kappa(\lambda, T, \rho)$ at the fixed density $\rho = 5 \times 10^{-3}$ g/cm^3 for the laser wavelength $\lambda = 1.06$ and 0.248 μm.

that the 0.248 μm radiation heats plasma more effectively at low temperatures, while at the temperature $T > 2$ eV absorption of the 1.06 μm radiation becomes more intensive.

3.2. Processes induced by the 1.06 μm laser radiation

Let us consider further the phase transition on the surface induced by the transmitted laser radiation. The time dependencies of the Mach number $Ma(t, r = 0)$, the surface temperature $T_c(t, r = 0)$, the saturated vapour pressure $P_{sat}(t, r = 0)$ and the plasma pressure $P_{pl}(t, r = 0)$ in the beam centre ($r = 0$, $z = 0$) for the laser pulse with $G_0 = 5 \times 10^8$ W/cm^2 are plotted in Fig. 4. The surface temperature that grows monotonically for the leading edge of the laser pulse lowers sharply at the instant of plasma formation and does not reach the critical value of 8000 K for aluminium, Fig. 4(a). Simultaneously the Mach number starts to decrease from the $Ma = 1$ level (the sonic velocity of the evaporated flux) to negative values $-1 < Ma < 0$ corresponding to the subsonic condensation. The vapour condensation is accompanied by the release of the heat of evaporation that compensates the conductive heat loss and, as a result, the temperature stabilizes at the level of approximately 4500 K. The two stages of the phase transition are also well seen in Fig. 4(b). For the pre-plasma stage, the saturated vapour pressure is several times higher and the necessary condition of evaporation is fulfilled $P_{sat} > P_{pl}$. After the plasma formation the counter-

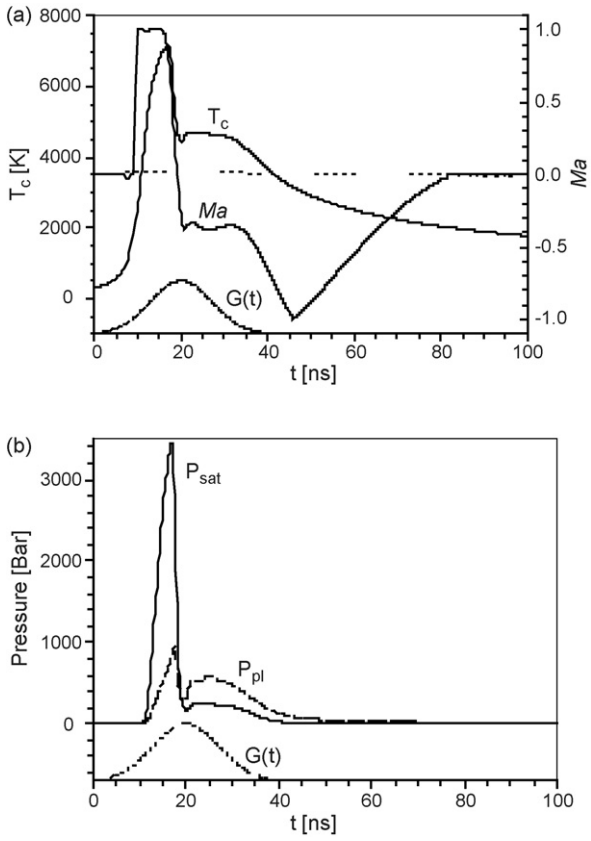

Fig. 4. Evolution of (a) the target surface temperature T_c and Mach number Ma, and (b) saturated vapour pressure P_{sat} and plasma pressure P_{pl} at the beam centre $r = 0$, $z = 0$ for the laser wavelength of 1.06 μm, $G_0 = 5 \times 10^8$ W/cm^2.

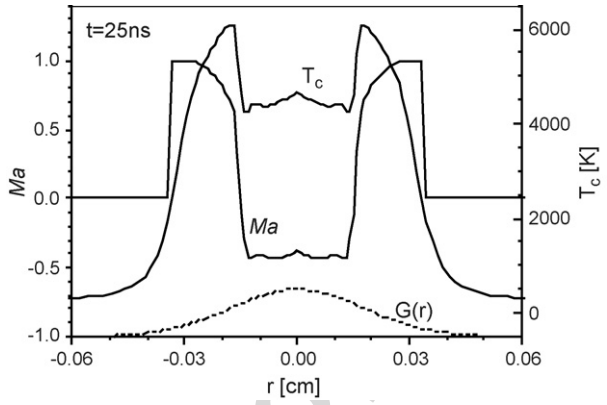

Fig. 5. Spatial distributions of the surface temperature $T_c(t = 25$ ns, $r)$ and the Mach number $Ma(t = 25$ ns, $r)$ for the laser wavelength of 1.06 μm, $G_0 = 5 \times 10^8$ W/cm^2.

pressure increases while P_{sat} drops down following the cooling of the surface, and on reaching the condition $P_{sat} < P_{pl}$ the vapour outflow becomes completely suppressed and condensation begins.

The phase transition in the entire irradiated region is illustrated by the dependencies of the surface temperature $T_c(r)$, and the Mach number $Ma(r)$ at $t = 25$ ns, Fig. 5. As it is seen the processes in the central and outer regions of the laser spot pass in different ways. The temperature curve has pronounced hollow in the central region $|r| < \approx r_f/2$ because in this region the laser intensity exceeds the plasma formation threshold and the laser flux reaching the target is substantially attenuated. In the outer region the plasma effect is much weaker and the target surface is heated much more intensively. Therefore, in the centre of the spot evaporation changes to condensation $Ma < 0$, while in the outer region $|r| > \approx r_f/2$ the intensive evaporation with $Ma \approx 1$ persists. As it was illustrated by the curve of the thickness of the removed material layer $H_v(r) = \int_0^{t_1} V_c(r, t')\,dt'$, $t_1 = 100$ ns, it is the outer region that gives the major contribution to the total mass removal.

3.3. Processes induced by the 0.248 μm laser radiation

The phase transition induced by the 0.248 μm laser radiation has a number of distinctions, Figs. 6 and 7. The instant of the plasma formation $t^* = 10$ ns is practically unnoticeable in the temperature plot $T_c(t)$, but is well seen in the $Ma(t)$ dependence, Fig. 6(a). The stage of the sonic evaporation, $Ma = 1$, turns out to be very short because of the early plasma formation. The most important difference as compared to the 1.06 μm radiation is that the evaporation does not stop after the plasma formation but continues even in an essentially subsonic regime $Ma \approx 0.1$ and condensation begins only after the end of the laser pulse. The corresponding pressure curves are shown in Fig. 6(b): the difference between the saturated vapour and plasma pressures $P_{sat} - P_{pl}$ substantially decreases but remains positive after the plasma formation.

The dependencies of the phase transition characteristics on r coordinate are shown in Fig. 7. The surface temperature T_c monotonically decreases from the centre to the boundary of the

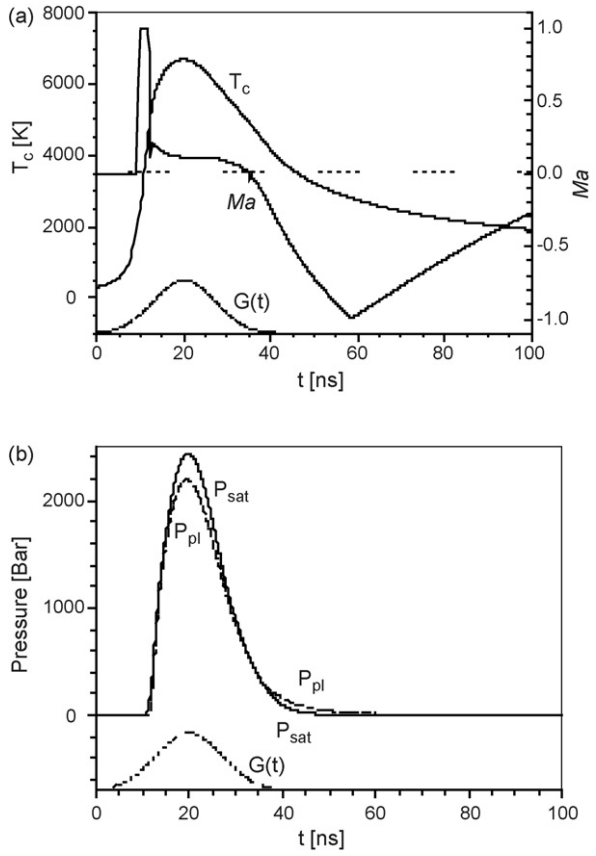

Fig. 6. Evolution of (a) the target surface temperature T_c and Mach number Ma, and (b) saturated vapour pressure P_{sat} and plasma pressure P_{pl} at the beam centre $r = 0$, $z = 0$ for the laser wavelength of 0.248 μm, $G_0 = 5 \times 10^8$ W/cm^2.

spot and has somewhat a more ''flat'' shape as compared to the one of the incident pulse, Fig. 7, curve T_c. The phenomenon is explained by a higher transmission of the plasma in the outer region of the spot that partially compensates the lower intensity of the incident pulse. The subsonic evaporation proceeds at approximately the same rate $Ma \approx 0.1$–0.15 throughout the spot region $|r| < r_f$, and the intensive evaporation with $Ma = 1$ is observed only in the outermost part of the irradiation zone, Fig. 7, curve Ma.

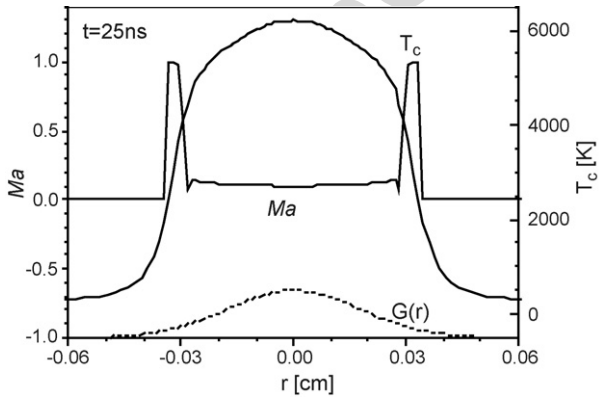

Fig. 7. Spatial distributions of the surface temperature $T_c(t = 25$ ns, $r)$ and Mach number $Ma(t = 25$ ns, $r)$ for the laser wavelength of 0.248 μm, $G_0 = 5 \times 10^8$ W/cm^2.

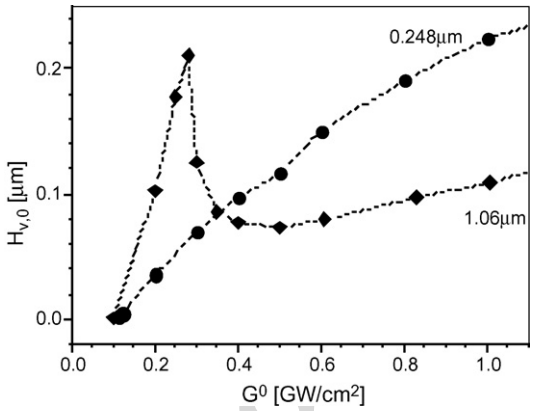

Fig. 8. Removed layer thickness in the beam centre vs. laser intensity $H_{v0}(G_0)$ predicted numerically for the laser wavelength of 1.06 and 0.248 μm.

3.4. Thickness of the removed layer

The thickness of the removed layer is likely the most often analysed quantity in laser ablation studies. The values of the removed layer thickness in the beam centre $H_{v,0} = H_v(r = 0)$ predicted for the 1.06 and 0.248 μm lasers with the different peak intensities $G_0 \in 10^8$–10^9 W/cm^2 are compared in Fig. 8. For the 1.06 μm radiation (diamonds) the curve has a pronounced maximum at the intensity of 2.5×10^8 W/cm^2, that corresponds to the plasma formation threshold at this wavelength. At lower intensities the plasma does not emerge and the thickness of the removed layer rapidly increases. A slow increase of the removed layer thickness is also observed at higher intensities in the plasma-controlled regime due to the removal of material near the beam boundaries and partially thanks to the subsonic evaporation resumed in the central part. For the 0.248 μm radiation, the vapour plasma is formed at nearly all the considered intensities, but it never completely stops evaporation (see Section 3.3). The respective $H_{v0}(G_0)$ curve demonstrates a monotonic growth with the smaller slope than the one for the 1.06 μm radiation in the before-plasma-formation regime.

4. Conclusion

The performed study allowed us to establish the following features of the phase transitions on the surface of an aluminium target and vapour plasma induced by the nanosecond radiation of the 1.06 and 0.248 μm laser with the intensity of 10^8–10^9 W/cm^2:

- The 1.06 μm irradiation leads to the formation of an optically dense plasma with the temperature of 5–10 eV that prevents further target heating; the evaporation stops but can occasionally resume at the final stage of the pulse; the evaporation proceeds non-uniformly in the spot area, the bulk of mass removal is attributive to the outer part of the spot above which the plasma is not formed and the sonic evaporation persists till the end of the action.
- For the 0.248 μm irradiation, the plasma appears shortly after the beginning of evaporation and screens the whole of the

spot area but remains colder and partially transparent transmitting 30–70% of the incident laser flux; the evaporation does not stop but continues in the subsonic regime with the Mach number of about 0.1 retarded by the high counter-pressure of the near-surface plasma layer.

Acknowledgment

This study was partly supported by RFBR grants nos 06-07-87191-a and 07-07-00045-a.

References

[1] Von Allmen, Laser-beam Interactions with Materials, Springer-Verlag, Berlin, 1987.
[2] R.E. Russo, X. Mao, S.S. Mao, Anal. Chem. 74 (2002) 70A.
[3] A. Gorbunov, Laser-assisted Synthesis of Nanostructured Materials, VDI Verlag, Dusseldorf, 2002.
[4] A.A. Samokhin, Effect of laser radiation on absorbing condensed matter, in: Proceedings of General Physics Institute USSR Academy of Science v. 13, Nova Science, New York, 1990.
[5] G.S. Romanov, V.K. Pustovalov, Izv. Akad Nauk BSSR Ser Fiz.-Mat. Nauk 4 (1967) 84.
[6] Ch.J. Knight, AIAA J. 17 (1979) 519.
[7] Y. Sone, S. Takata, F. Golse, Phys. Fluids 13 (2001) 324.
[8] M. Aden, E. Beyer, G. Herziger, H. Kunze, J. Phys. D: Appl. Phys. 25 (1992) 57.
[9] V.I. Mazhukin, A.A. Samokhin, Sov. J. Quantum Electron. 14 (1984) 1608.
[10] Ch.J. Knight, AIAA J. 20 (1982) 950.
[11] S.H. Jeong, R. Greif, R.E. Russo, Appl. Surf. Sci. 127–129 (1998) 177.
[12] A.V. Gusarov, I. Smurov, J. Appl. Phys. 97 (2005) 014307.
[13] R. Kelly, A. Miotello, Nucl. Instrum. Meth. Phys. Res. B 91 (1994) 682.
[14] Z. Chen, A. Bogaert, J. Appl. Phys. 97 (2005) 060305.
[15] G.S. Romanov, Yu.A. Stankevich, Fiz. Khim. Obrabot. Mater. 2 (1981) 15.
[16] A. Vertes, R.W. Dreyfus, D.E. Platt, IBM J. Res. Dev. 38 (1994) 1.
[17] J.R. Ho, C.P. Grogoropoulos, J.A.C. Humphrey, J. Appl. Phys. 79 (1996) 7205.
[18] T.E. Itina, J. Hermann, P. Delaporte, M. Sentis, Phys. Rev. E, 66 (2002) 066406/1.
[19] V.I. Mazhukin, G.A. Pestryakova, Dokl. Akad. Nauk SSSR 278 (1984) 843.
[20] V.I. Mazhukin, V.V. Nossov, I. Smurov, Thin Solid Films 453–454 (2004) 353.
[21] V.I. Mazhukin, V.V. Nossov, J. Quantum Electron. 35 (2005) 454.
[22] D.I. Rosen, J. Mitteldorf, G. Kothandaraman, A.N. Pirri, E.R. Pugh, J. Appl. Phys. 53 (1982) 3190.
[23] I. Horn, M. Guillong, D. Gunther, Appl. Surf. Sci. 182 (2001) 91.
[24] V.I. Mazhukin, V.V. Nossov, I. Smurov, J. Appl. Phys. 90 (2001) 607.
[25] G.S. Romanov, K.L. Stepanov, M.I. Sirkin, Opt. Spectrosc. (USSR) 53 (1982) 381.
[26] Ya.B. Zeldovich, Yu.P. Raizer, Physics of Shock waves and High Temperature Hydrodynamics Phenomena V. I, II, Academic, New York, 1966.
[27] K. Aoki, Y. Sone, T. Yamada, Phys. Fluids A 2 (1990) 1867.
[28] A.A. Samarskii, Teoriya raznostnykh skhem, Nauka, Moscow, 1977.
[29] V.I. Mazhukin, I. Smurov, G. Flamant, J. Comp. Phys. 112 (1994) 78.
[30] I.S. Grigoriev, E.Z. Meilikhov, Handbook of Physical Quantities, CRC Press, New York, 1997.
[31] I.W. Boyd, Laser Processing of Thin Films and Microstructures, Springer-Verlag, Berlin, 1987.